

Original article

The impact of geological heterogeneity on horizontal well-triplet performance in CO₂-circulated geothermal reservoirs

Mingjie Chen¹*, Aliya Al-Saidi^{1,2}, Ali Al-Maktoumi^{1,3}, Azizallah Izady¹

¹Water Research Center, Sultan Qaboos University, Muscat 123, Oman

²Department of Chemical and Petroleum Engineering, Sultan Qaboos University, Muscat 123, Oman

³Department of Soils, Water and Agricultural Engineering, Sultan Qaboos University, Muscat 123, Oman

Keywords:

Geothermal production
CO₂ circulation
geological heterogeneity
correlation length
horizontal well
closed reservoir

Cited as:

Chen, M., Al-Saidi, A., Al-Maktoumi, A., Izady, A. The impact of geological heterogeneity on horizontal well-triplet performance in CO₂-circulated geothermal reservoirs. *Advances in Geo-Energy Research*, 2022, 6(3): 192-205.
<https://doi.org/10.46690/ager.2022.03.03>

Abstract:

CO₂ circulated geothermal production can be integrated with CO₂ geological sequestration as a utilization method to offset cost. Investigation of heterogeneity impact is limited to CO₂ sequestration and its effect on CO₂ circulation and associated heat recovery is unclear. This study is aimed to improve the understanding of this problem by numerical experiments. A set of spatially correlated heterogeneous porosity fields is generated using a variety of geostatistical parameters, i.e., variance, correlation lengths, anisotropy and azimuth. Heterogeneous fields of intrinsic permeability and initial/residual water saturation are derived from porosity using equations regressed from a field dataset. Twenty combinations of injection pressure and well space obtained by Latin-Hypercube sampling are deployed in each heterogeneous field, generating a suite of numerical geothermal reservoir models. Performance indicators, including lifespan, net stored CO₂, produced heat flux, and total recovered heat energy in lifespan, are calculated from each model simulation. The simulation results suggest that geologic heterogeneity could develop high-permeable CO₂ flow paths, causing bypass of the hot low-permeable zones, shortened lifespan and reduced total recovered heat energy. Depending on the azimuth, anisotropy can create either flow barriers or preferential flow paths, increasing or decreasing heat sweeping efficiency. The relative angle between horizontal wells and the axis of maximum continuity of the heterogeneity can be optimized to maximize heat recovery efficiency. These finds provide useful insights of interplay between geological heterogeneity, well placement and operation of CO₂ circulated geothermal production.

1. Introduction

In the past 50 years, drastic increase of CO₂ emission to atmosphere, primarily from fossil fuel consumption, has caused notable climate change and environmental issues globally (Abas and Khan, 2014). As a strategic mitigation approach, CO₂ geological storage has been investigated and implemented all around the world in the past two decades (IPCC, 2005; Shaffer, 2010; GCCSI, 2014; Mac Dowell et al., 2017; Chen et al., 2020; Xu et al., 2022). As a utilization approach supplementing sequestration, CO₂ can act as a working fluid to extract geothermal energy. This CO₂-circulated heat harvest

has been extensively studied and demonstrated more efficient than traditional water-circulated method (Randolph and Saar, 2011; Adams et al., 2015; Sun et al., 2018; Chen et al., 2022). During CO₂ circulation, the injected cold CO₂ is heated as it migrates towards production wells. The hot CO₂ extracted from the production wells goes through a CO₂ gas turbine generator to produce electricity on ground surface. The cooled CO₂ is then re-injected back to the geothermal reservoir. CO₂ generates a strong thermosiphon through the injection and production wells because of the drastic changes of CO₂ density with pressure (Atrens et al., 2009; Adams et al., 2014). As

a result, no pumping is often required for CO₂ extraction from the production wells. A portion of the injected CO₂ will never be recycled and instead be permanently stored in the subsurface formation. Hence, besides energy production, the systems have the supplemental benefit of CO₂ storage.

A few studies have examined the impact of formation heterogeneity on traditional water-circulated geothermal production. The impact of facies heterogeneity on the doublet performance of a low-enthalpy geothermal fluvial reservoir was investigated by Crooijmans et al. (2016) using model simulations. They found that both water extraction rates and net-to-gross ratios determine the lifespan of the geothermal reservoirs. Heterogeneity causes overestimation of lifespan especially in high net-to-gross regions. Connectivity of the heterogeneous facies in the Nieuwerkerk formation was particularly studied by Willems et al. (2017). Their results suggest neglect of heterogeneity could significantly underestimate the geological risks of doublet, which should be placed in parallel to the paleo flow direction in order to maximize heat recovery. The work by Liu et al. (2019) revealed that the long correlation length of the heterogeneous fields could create preferential flow channels, causing earlier cold-water breakthrough. Barbaei and Nick (2019) conducted a comprehensive numerical experiment to systematically investigate the interplay of formation heterogeneity and doublet spacing and discharge. Nine performance metrics are defined to measure the geothermal production under a suite of heterogeneity scenarios generated by various geostatistical model parameters. They concluded that heterogeneity anisotropy could cause either positive or negative impact on the lifespan. Same doublet spaces should be placed to minimize the impact of heterogeneity. Most of the studies reviewed above deal with vertical well doublet placement in deep thick saline aquifers. Depleted oil/gas reservoirs are considered good candidates for CO₂ sequestration and subsequent CO₂ circulation for geothermal production. These reservoirs are usually characterized by thin, low-permeable fault blocks, and horizontal wells have been applied to improve sweeping efficiency during water flooding or CO₂ enhanced oil recovery (Zhao et al., 2012). The influences of rock heterogeneity on geothermal harvest using horizontal wells in this type of reservoir have never been studied and remain unclear.

With CO₂ sequestration projects being implemented in tens of sites, impact of heterogeneity on CO₂ migration, storage and trapping are being investigated by numerical simulations, laboratory and field experiments, from pore-scale to reservoir-scale (e.g., Dai et al., 2014; Rasheed et al., 2020; Ershadnia et al., 2022). The latest advances on this topic can be found in the works by Harris et al. (2021), Ren et al. (2021), Sohal et al. (2021) and Williams and Chadwick (2021). Whereas, none of them have been focused on heterogeneity effects on CO₂ circulated geothermal production within CO₂ plume developed during sequestration. As the first attempt to address this knowledge gap, we carry out a suite of numerical experiments by placing a horizontal well-triplet in a thin, low-permeable formation to circulate CO₂ and harvest heat energy, based on a fault-block reservoir in Daleel oil field in north Oman. While mean value is kept the same, the variance,

correlation lengths in x and y , azimuth of the spatial correlated random fields of reservoir properties are varied to generate a set of heterogeneity scenarios. For each scenario, a suite of injection scheme and well space are designed to investigate the combined impact of heterogeneous porous media and horizontal well-triplet operation on the CO₂ circulation and heat extraction.

2. Methodology

2.1 CO₂-circulated geothermal reservoir model

The numerical model simulations are carried out by using Non-isothermal Unsaturated-saturated Flow and Transport (NUFT), which is capable of simulating multi-phase multi-component heat/mass flow and transport in porous media (Nitao, 1998; Hao et al., 2012). NUFT is incorporated with reliable equations of state for CO₂: Thermophysical properties, including density, compressibility, and viscosity, are determined dynamically by the correlation of Span and Wagner (1996) and Fenghour et al. (1998), respectively. In the past 10 years, NUFT has been successfully applied in many CO₂ related underground reservoir studies (Buscheck et al., 2012, 2013, 2014; Saar et al., 2015; Chen et al., 2020, 2021, 2022).

The reservoir system in this study is based on the fault block B of Daleel oil field in North Oman (Abbaszadeh, 2000; Zhang et al., 2007; Zhao et al., 2012), where highest subsurface temperature is found in a hydrogeological survey by Al-Lamki and Terken (1996). The carbonate formation is characterized by high porosity, low permeability, and moderate heterogeneity. The model domain is a three-dimensional (3D) rectangle with 2.5 km × 3 km × 20 m in x , y , and z directions (Fig. 1). The domain is discretized by a xyz block of 50 m × 50 m × 1 m uniformly, leading to a model mesh system consisting of 50 × 60 × 20 = 60,000 grid cells. The top domain is 1.5 km deep, ground surface temperature is assumed 30 °C based on the weather conditions in the study area, and vertical geothermal gradient is set as 40 °C/km. Initial pressures and temperatures are calculated and assigned to each cell of the domain according to their depth by using these reference data and hydrostatics. All the boundaries are completely sealed by caprock, bedrock, and faults and assumed impermeable to fluids flow. A geothermal heat flow of 50 mW/m² is specified on the bottom boundary (Schütz et al., 2018). Porosity, permeability, initial water saturation, and residual water saturation used in van Genuchten models calculating capillary pressure and phase relative permeability are considered spatially heterogeneous to be discussed in the next section. Other rock and fluid properties are treated homogeneous. Density and compressibility of the rock are 2,650 kg/m³ and 4.5 × 10⁻¹⁰ Pa⁻¹. Rock specific heat and thermal conductivity are assumed 1,000 J/(kg·°C) and 2.1 W/(m·°C). Brine salinity is found to be 180 ppt (kg/kg in parts per thousand) from field measurements. Van Genuchten parameter α and m are set as 5.1 × 10⁻⁵ Pa⁻¹ and 0.46, respectively.

A horizontal well triplet is deployed for this thin reservoir. As shown in Fig. 1, three 1-km long wells are placed in parallel between $y = 1,000$ - $2,000$ m along y -axis, with the injection

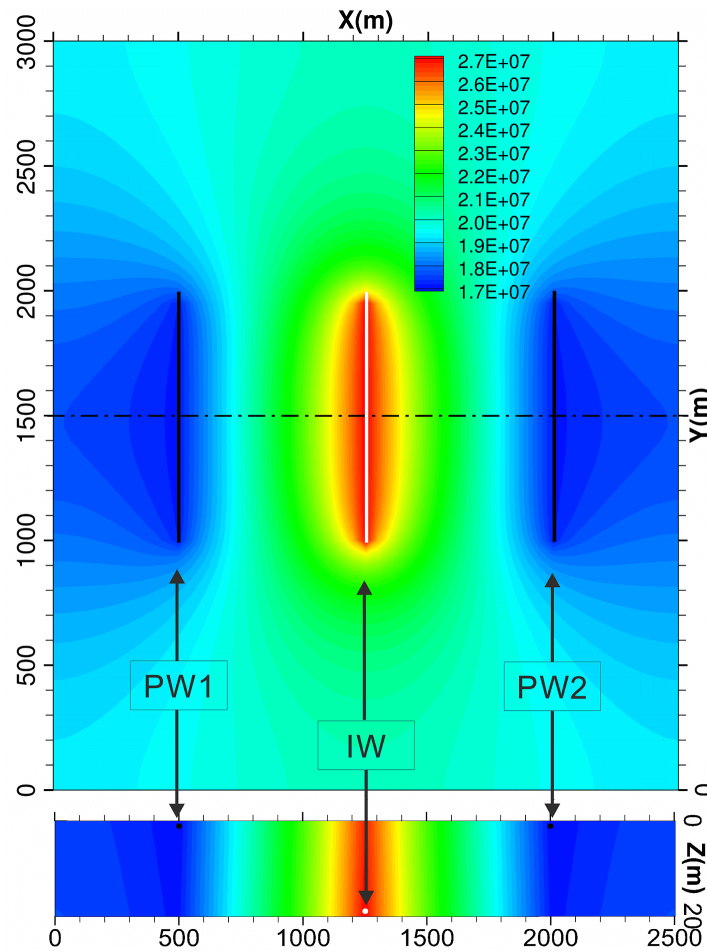


Fig. 1. Top XY and middle XZ slices showing the model domain dimensions and well placement. The background map is the pressure (Pa) distribution in 10 years of simulation for the homogeneous reservoir with $dP = 10$ MPa, $L_w = 750$ m. The scale of Z is exaggerated by 20 to XY.

well (IW) on the bottom in the middle $x = 1,250$ m, and two production wells (PW1, PW2) on the top and symmetric to IW. The x distance of PW1/PW2 to IW is referred as well space (L_w), which is a key decision parameter in geothermal production. The pressure is fixed constant as initial pressure at PW1 and PW2, and an overpressure (dP) is applied at IW, increased from 0 to the specified value in the 1st year and remains constant afterwards. CO₂ is driven by pressure gradient between IW and PW, which is affected by L_w and dP . A suite of scenarios is designed to investigate the interplay between rock heterogeneity and operational parameter $L_w - dP$, as well as their impacts on performance of geothermal production.

2.2 Heterogeneous scenarios

Heterogeneous porosity is modeled as spatially correlated 3D random field, which is generated using a Matlab code based on discrete Fourier transformation (Cirpaka, 2003). As specified in Table 1, six heterogeneous scenarios (S1-S6) with different variance (σ^2), x and y correlation length (CL_x , CL_y), or azimuth angle are designed, each scenario with eight equally generated realizations. In all the realizations, the mean of porosity is fixed as 0.25, and z correlation

length (CL_z) is fixed as 1.0 m. S1 can be considered as the baseline heterogeneous cases, with $CL_x = CL_y = 800$ m and $\sigma^2 = 0.002$, adapted from the geostatistical study of the same site by Abbaszadeh et al. (2000). The parameters changed from S1 is marked in red fonts for S2-S6 (Table 1). S2 with doubled variance ($\sigma^2 = 0.004$) is designed to investigate how stronger heterogeneity would affect the reservoir performance. S3-S6 with quarter CL_x or CL_y of S1 or 45° angle to horizontal wells are expected to reveal the effect of spatial correlation length and anisotropic heterogeneity on the horizontal well placement during geothermal production. Homogeneous scenario (S0) is also simulated as the reference cases. The 1st realization of porosity fields for S1-S6 are shown in Fig. 2. It is seen that differences of σ^2 , CL_x , CL_y , and azimuth angle are clearly demonstrated in the six generated 3D random fields.

Rock intrinsic permeability (k) and initial water saturation (S_{wi}) are treated heterogeneous too, and can be derived from porosity (ϕ) by relationships constructed from core data as following (Abbaszadeh et al., 2000):

$$k = 192 \frac{\phi}{(1 - \phi)^2} \quad (1)$$

Table 1. Simulation scenarios of the homogeneous (S0) and six heterogeneous (S1-S6) reservoirs*.

| Scenarios | Variance σ^2 | X Corr. Length CL_x (m) | Y Corr. Length CL_y (m) | Azimuth (degree) |
|-----------|--|---------------------------|---------------------------|------------------|
| S0 | Homogeneous properties using mean parameter values | | | |
| S1 | 0.002 | 800 | 800 | 0 |
| S2 | 0.004 | 800 | 800 | 0 |
| S3 | 0.002 | 200 | 200 | 0 |
| S4 | 0.002 | 800 | 200 | 0 |
| S5 | 0.002 | 200 | 800 | 0 |
| S6 | 0.002 | 200 | 800 | 45 |

*Eight realizations of the porosity field are generated for S1-S6 using the parameters in the table. Permeability and initial/residual water saturation ($S_{wi} = S_{wr}$) of each grid cell are derived from porosity according to Eqs. (1) and (2). Porosity mean is set as 0.25, and Z correlation length CL_z is fixed as 1.0 m in generating realizations. For S0, uniform values of porosity = 0.25, permeability = 5.34 mD, and $S_{wi} = 0.3$ are assigned for every grid cell.

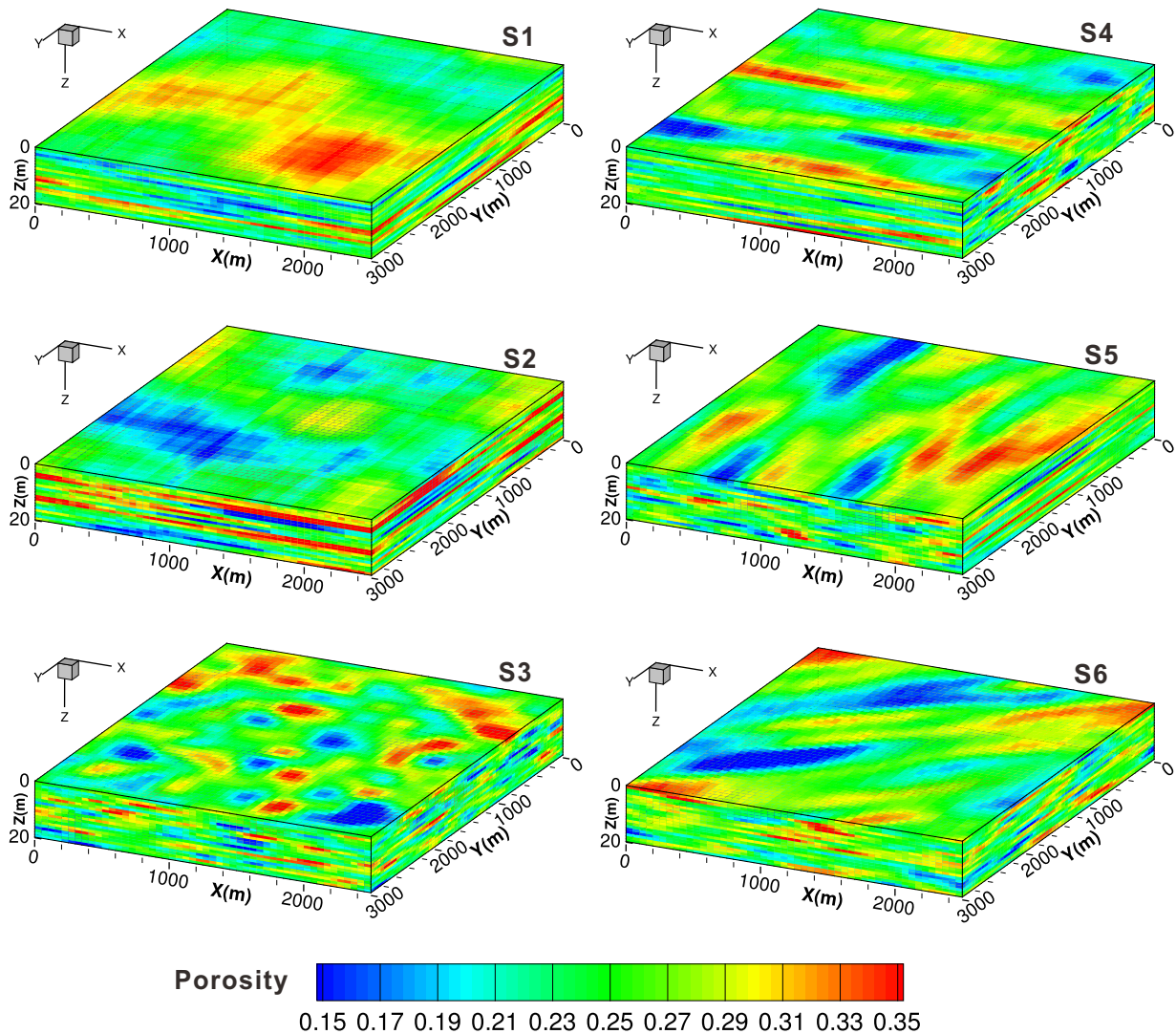


Fig. 2. The 1st realization of porosity field for S1-S6. The scale of Z is exaggerated by 20 to XY .

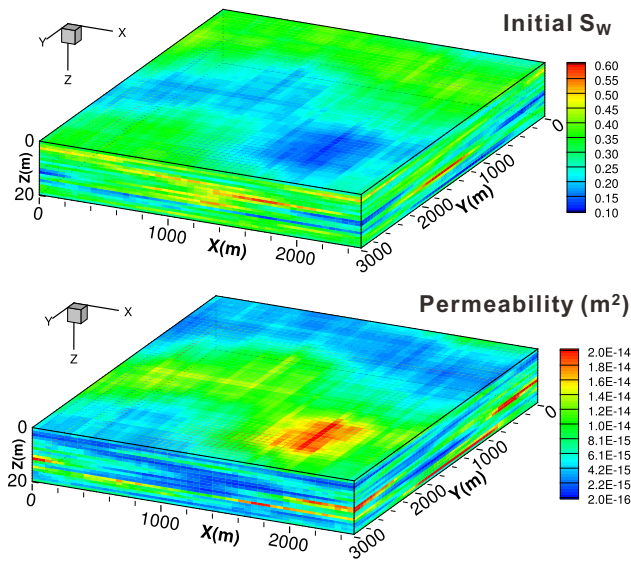


Fig. 3. The random fields of permeability and initial/residual water saturation derived from the porosity field of the 1st realization of S1 using Eqs. (1) and (2), respectively. The scale of Z is exaggerated by 20 to XY.

Table 2. Latin-Hypercube samples of overpressure ($dP = 5\text{--}15$ MPa) and well space ($L_w = 500\text{--}1,000$ m) used to generate 20 models of S0 and each of the 8 realizations of S1-S6.

| $dP\text{-}L_w$ Sample# | Overpressure dP (MPa) | Well space L_w (m) |
|-------------------------|-------------------------|----------------------|
| 1 | 5.19 | 983 |
| 2 | 8.59 | 544 |
| 3 | 13.20 | 855 |
| 4 | 12.31 | 900 |
| 5 | 14.20 | 639 |
| 6 | 6.15 | 921 |
| 7 | 11.20 | 502 |
| 8 | 10.84 | 809 |
| 9 | 8.29 | 594 |
| 10 | 8.91 | 694 |
| 11 | 10.42 | 668 |
| 12 | 11.77 | 619 |
| 13 | 9.56 | 560 |
| 14 | 7.28 | 843 |
| 15 | 13.56 | 707 |
| 16 | 14.57 | 945 |
| 17 | 7.63 | 765 |
| 18 | 9.34 | 793 |
| 19 | 12.94 | 963 |
| 20 | 6.66 | 729 |

$$S_{wi} = 85 \lg \left(\frac{1}{\phi} - 1 \right) - 10 \quad (2)$$

Since only two fluids, water and CO_2 , are considered in this study, the initial CO_2 saturation is $1 - S_{wi}$. As the initial CO_2 plume results from geological sequestration or enhanced oil recovery, it is reasonable to consider residual water saturation (S_{wr}) as the same value of S_{wi} in every grid cell. Consequently, capillary pressure and fluid relative permeability determined by van Genuchten models, which are functions of S_{wr} , are also heterogeneous in model simulations. Fig. 3 presents an example of k and S_{wi} derived from ϕ of the 1st S1 realization using Eqs. (1) and (2). It is seen that k and S_{wi} is positively and negatively correlated to ϕ in general, respectively.

To investigate the interplay of operation scheme and heterogeneous scenarios, 20 pairs of $dP\text{-}L_w$ are sampled in their ranges using Latin-Hypercube approach (McKay et al., 1979), as shown in Table 2. For S0 and each of eight realizations of S1-S6, the 20 $dP\text{-}L_w$ samples are used to generate 20 NUFT models, resulting in $20(dP\text{-}L_w \text{ for S0}) + 20(dP\text{-}L_w) * 8(\text{Realizations}) * 6(\text{S1-S6}) = 980$ NUFT models totally. The models are distributed to a number of computing nodes of clusters at Sultan Qaboos University to run simultaneously, and each model cost about 2 hours to simulate to 100 years. Four performance indicators are calculated from the model outputs, including:

- 1) Lifespan (years): The simulation time when the temperature of produced fluids drops below 80°C from initial 90°C . The temperature is averaged from fluid temperatures of both PW1 and PW2.
- 2) Stored CO_2 (Mt, Mega tonnes): The net injected CO_2 mass (injected - produced) within lifespan. Although the initial reservoir is full saturated by CO_2 (initial $S_{\text{CO}_2} = 1 - S_{wr}$), more pore space could be freed mainly by compressible rock and fluids under overpressure, as well as minor co-produced brine.
- 3) Produced heat flux (MW, Mega Watts): Produced CO_2 heat flux averaged in lifespan years.
- 4) Produced total heat (10^{15} J, Joules): Cumulative heat energy from produced CO_2 in lifespan.

Average values of these four indicators from the eight realizations of S1-S6 are examined against S0, not only in 20 $dP\text{-}L_w$ sample points but also in continuous $dP\text{-}L_w$ two-dimensional (2D) parameter space using response surface method (Chen et al., 2021, 2022).

To demonstrate spatiotemporal behaviors of the studied geothermal operation, additional seven simulations are conducted for S0 and the 1st realization of S1-S6 with $dP = 10$ MPa and $L_w = 750$ m.

3. Results and discussion

3.1 Spatiotemporal behaviors of geothermal reservoirs

3.1.1 Time series of reservoir state

The temporal behavior is similar for all the scenarios; therefore, we take S1 and S2 as an example for interpretation.

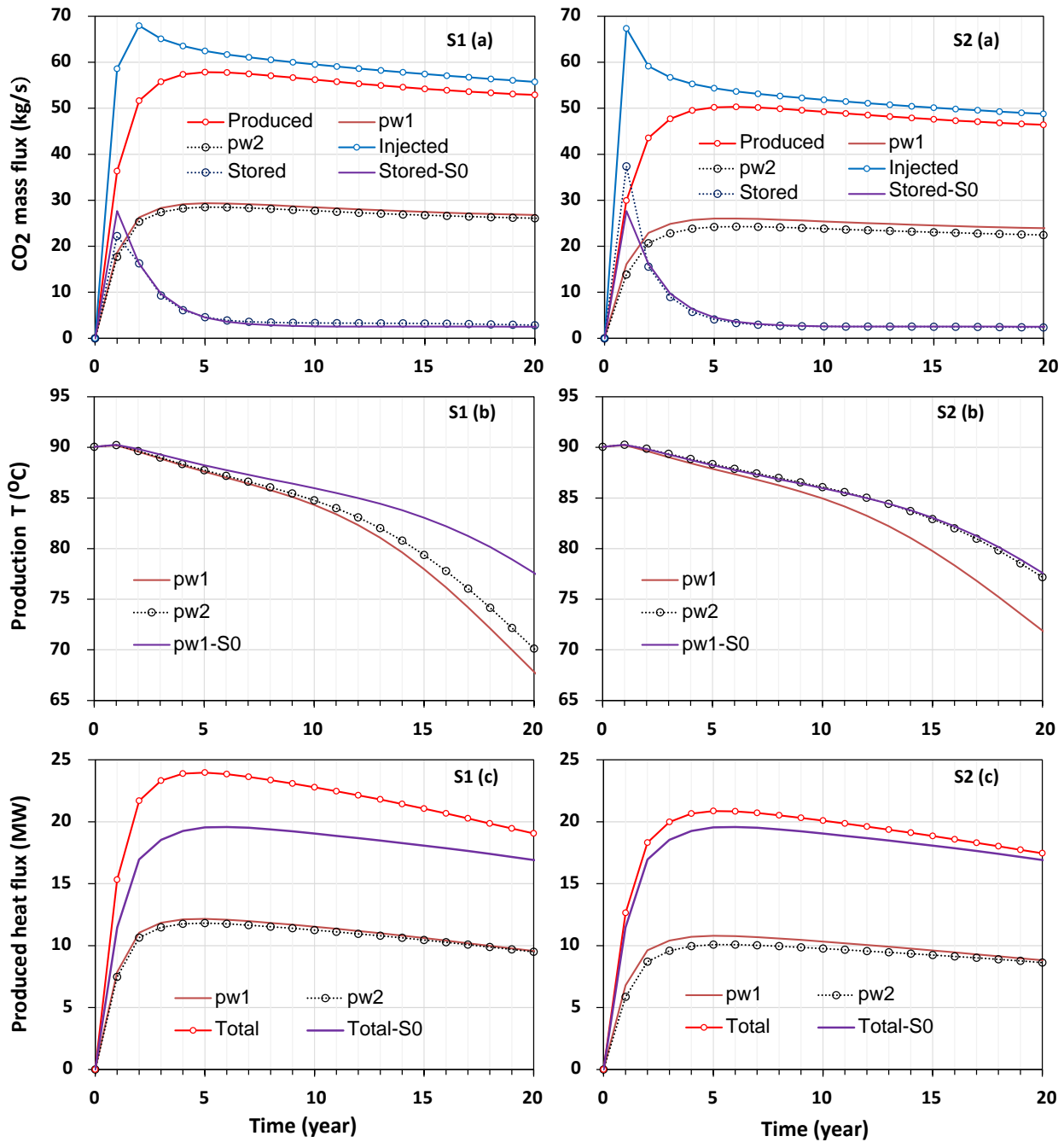


Fig. 4. Comparison of (a) CO₂ mass flux, (b) temperature, and (c) produced heat flux in the 1st realization of S1 and S2 against S0 with $dP = 10$ MPa, $L_w = 750$ m. In figure (a), legend Produced = pw1 + pw2, and Stored = Injected – Produced.

Fig. 4 shows the 20 years of CO₂ mass flux, produced temperature and heat flux for the 1st realization of S1 and S2 with $dP = 10$ MPa and $L_w = 750$ m. Stored CO₂ flux, produced CO₂ temperature and heat flux from S0 are also plotted as the reference case. Unlike the heterogeneous scenarios, produced fluid mass, heat, and temperature from PW1 and PW2 are the same in S0, since they are symmetrically placed on each side of IW.

As shown in Fig. 4(a), CO₂ injection rates in S1 and S2 soar in the 1st year, when the overpressure at IW linearly increases from 0 to 10 MPa. The rates then gradually decrease

afterwards, as overpressure remains constant. Meanwhile, CO₂ starts to be produced from PW1 and PW2 quickly, but not as quick as injection in the 1st year. Produced rates continue to increase smoothly and reach peak in around 5th year, and then slowly decrease almost in parallel to injection rate curve. The stored CO₂, i.e., the gap between injected and total produced rate, increases sharply in the 1st year, and then falls drastically too, but remains almost constant after 5 years. These results indicate it needs 5 years for CO₂ circulation to stabilize in response to the increase of IW overpressure in the 1st year. Although the pressure gradient between IW and PW remains

constant after 1 year, it takes much longer time for fluids flow to adapt the pressure field change. Both injected and produced rates are higher in S1 than those in S2 overall, suggesting the effective permeability in the sweeping area is higher in S1. There are lower permeability barriers between IW and PW in S2 due to the stronger heterogeneity (lower low and higher high k). It is interesting that in the 1st year, injected rate is higher but produced rate is lower in S2 than those in S1, leading to a higher storage rate (37.39 vs. 22.25 kg/s). This result indicates k is higher near IW and lower near PW in S2 than in S1. The larger gap of produced rate between PW1 and PW2 in S2 than that in S1 also demonstrates the larger difference of k between the two sweeping areas in S2 with stronger heterogeneity. In addition, the higher produced rate in PW1 suggests higher effective k in IW-PW1 area than that in the other side. Whereas heterogeneity has a minor impact on the stabilized storage rate, which is almost the same in S0, S1 and S2 after 5 years (about 3 kg/s). It is because pressure is the dominant factor affecting the storage rate by compressing rock and fluids. As the stabilized pressure fields are the same in all the scenarios, the stabilized storage rate will not differ a lot.

Temperature (T) profiles of the two production wells are presented in Fig. 4(b) for S0, S1, and S2. As T in the both production wells is the same in S0, only T in PW1 is plotted. As expected, T falls gradually with the CO₂ circulation, and the decline rate is determined by the production rate: The higher the production rate, the faster the decline of T . In S1, T in PW1 declines faster than that in PW2, and both are faster than two PWs in S0 due to the different production rates in these wells. Similar explanation is applicable to the patterns of T profiles in S2. The larger gap between PW1 and PW2 in S2 than that in S1 is also caused by the larger gap of production rate in the two wells of S2. T is also used as the criteria to determine the lifespan of the geothermal reservoir in this study. The lifespan for the three simulations in S0, S1, and S2 is 18, 14, and 16.5 years, respectively, as 80 °C is set as the cutoff temperature.

Produced heat flux is calculated as a product of CO₂ mass flux and specific enthalpy, which is a function of pressure and temperature. As pressure field is the same in all the scenarios, the difference of heat flux is determined by that of mass flux and temperature. As shown in Fig. 4(c), the heat flux profiles follow similar patterns of mass flux in each well, but drop a little faster in later times when T declines more significantly.

3.1.2 Spatial distribution of temperature

Reservoir pressure distribution is similar in all scenarios; however, the fluid spread and the resulted temperature spatial distribution are significantly affected by formation heterogeneity. Figs. 5 and 6 present T distribution on top XY plane and middle XZ cross-section after 10 years of CO₂ circulation in S0-S6. As shown in Fig. 5, the horizontal distribution is perfectly IW-symmetric in S0, but shows different patterns in S1-S6. The plume is distorted by the heterogeneous k field: Enhanced in high k and blocked in low k area. The low- T plume spreads farther in S1 than S0, indicating more cold-CO₂ passed the higher k area by the 10th year, as shown in Fig.

4(a). The plume in S2 demonstrates stronger heterogeneity: CO₂ flows much more preferentially through the lower area than the upper area, especially in PW1-IW region (left side of IW).

The effects of correlation length of the random fields are demonstrated in S3-S6. The T plume in S3 shows smaller-scale preferential paths due to the shorter CL_x and CL_y than S1 (200 m vs. 800 m). S4 is characterized by high and low permeable lens in parallel to x -axis ($CL_x = 800$ m, $CL_y = 200$ m) and CO₂ flow direction as shown in Fig. 2. As a result, T plume is prominently zigzag along y -axis (Fig. 5). In contrast, the lenses in S5 are in parallel to y -axis ($CL_x = 200$ m, $CL_y = 800$ m) and horizontal wells, and the y -scale is close to the length of the wells (800 vs. 1000 m). Hence, the low- k lenses could serve as flow barriers between PW and IW. It seems that such barriers happen to exist between PW1 and IW in the 1st realization of S5, as low- T spread is more significantly restricted compared to the other side (Fig. 5). The lenses in S6 are rotated by 45° (azimuth) from S5 and in parallel to diagonal in XY plane. The resulted T plume is between that from S4 and S5.

Although the reservoir is only 20-m thick, the correlation length in z is as short as 1 m in all the scenarios. The z grid space of the model is also specified as 1 m in order to demonstrate the spatial-correlated heterogeneity in z direction. As shown in Fig. 6, the effects of z -heterogeneity are demonstrated in T plume in XZ cross-section in middle y for S1-S6, but there is no big difference of vertical distribution between them, since CL_z is fixed as 1 m in all of them.

3.2 Performance of geothermal production

Spatiotemporal patterns of the geothermal reservoir in S0 and the 1st realization of S1-S6 are discussed in the last section. The realizations equally generated by the same geostatistical model parameters, including mean, variance, correlation length, and azimuth, can differ considerably. Although the values and heterogeneous scales are similar, the locations of high and low values are randomly assigned and could lead to significant differences in the model outputs from one realization to another one. As shown in Fig. 7, the performance indicators from the eight realizations for each dP - L_w sample can vary a lot, and their values are overlapped between some samples. Therefore, mean indicator values of the eight realizations for each dP - L_w sample are used to represent the heterogeneous scenarios S1-S6 in Figs. 8 and 9 to be discussed in this section. Fig. 8 shows the 2D response surfaces of the four indicators versus dP and L_w in S0, S1 and S2 only, as the distribution patterns are similar in other scenarios. Fig. 9 compares these indicators between S0-S6 for every dP - L_w sample.

3.2.1 Lifespan

Lifespan is determined as the operation time until the temperature averaged in PW1 and PW2 drops below 80 °C. The faster the cold CO₂ arrives PW, the shorter the lifespan. CO₂ circulation flux is determined by IW-PW pressure gradient and well space L_w . As the pressure in PW is fixed, overpressure dP

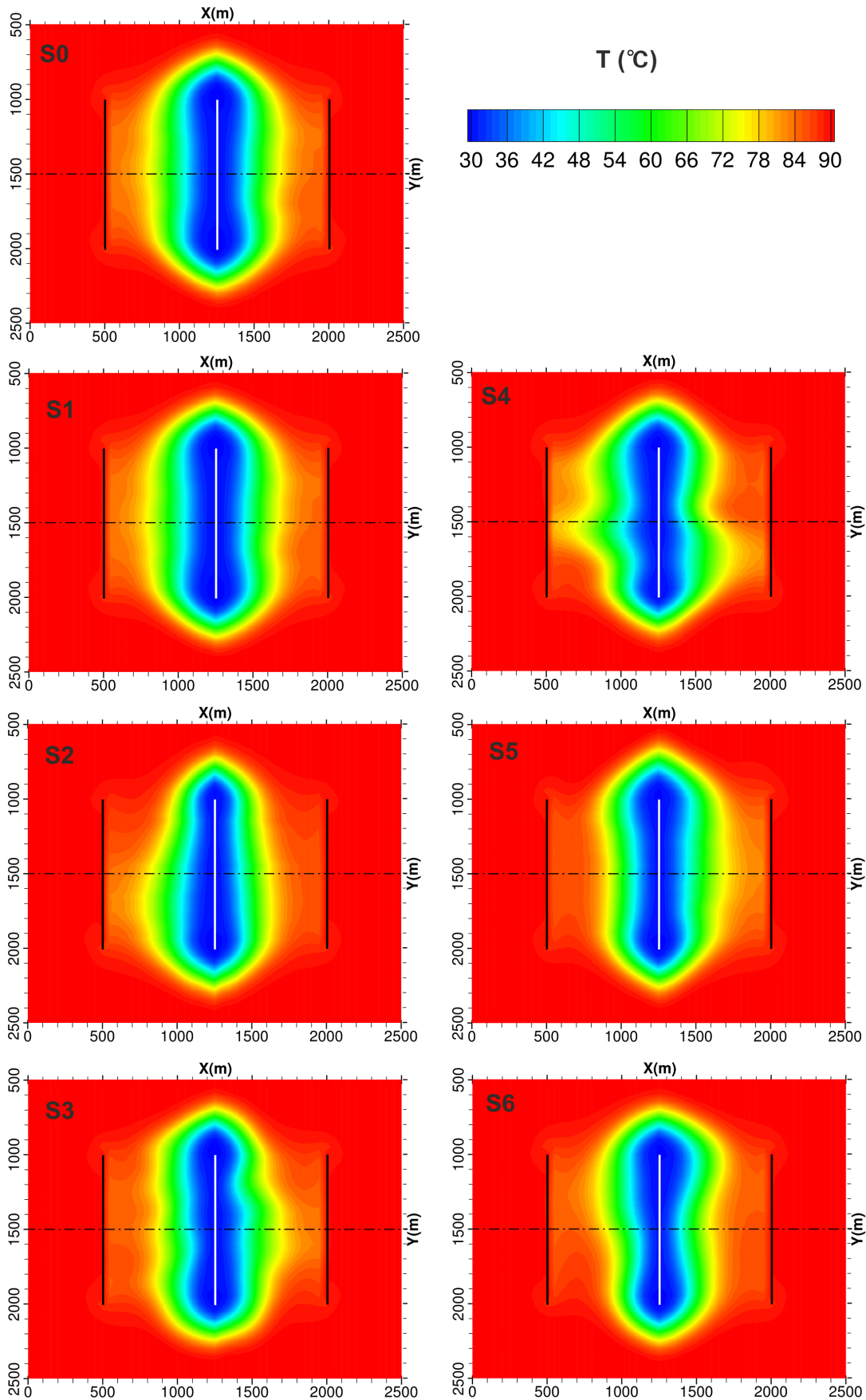


Fig. 5. Top XY slice showing the temperature distribution in 10 years of simulation for S0 and the 1st realization of S1-S6 with $dP = 10$ MPa, $L_w = 750$ m. The white and two black solid lines represent IW and 2 PWs (PW1 and PW2), respectively.

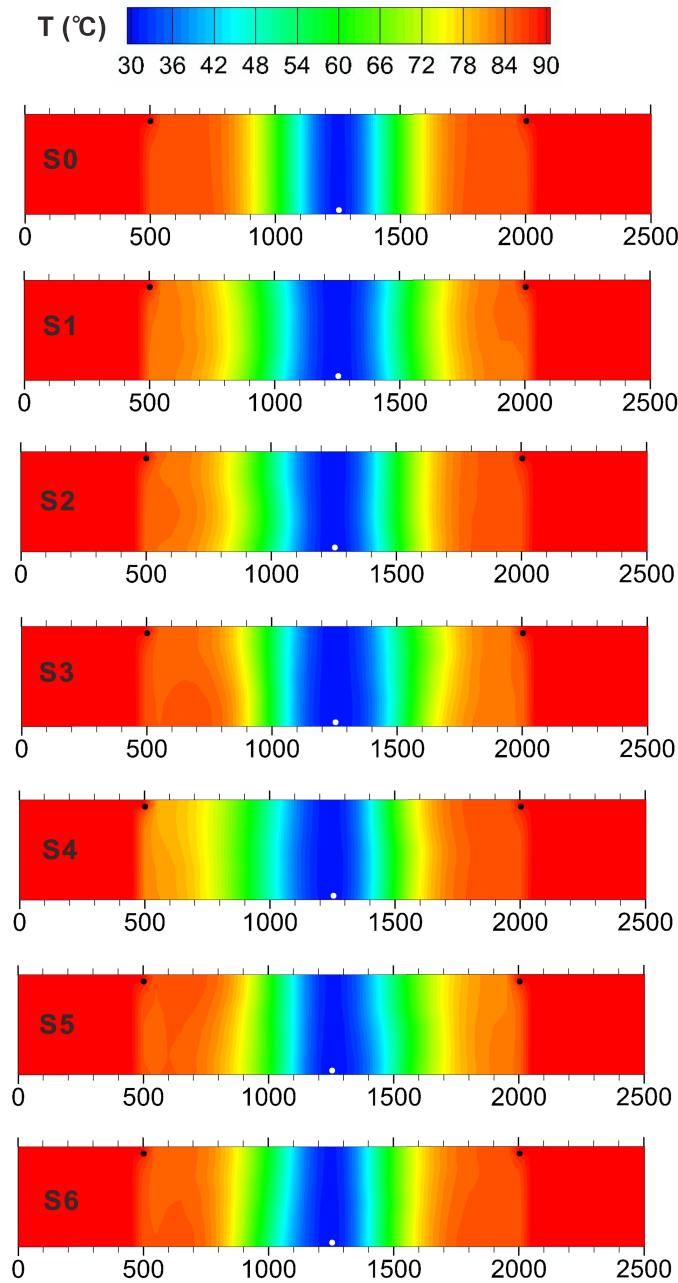


Fig. 6. XZ cross-section in $Y = 1500$ m showing the temperature distribution in 10 years of simulation for S0 and the 1st realization of S1-S6 with $dP = 10$ MPa, $L_w = 750$ m. The scale of Z is exaggerated by 20 to X. The white and two black solid circles represent IW and 2 PWs (PW1 and PW2), respectively.

in IW determines the inter-well pressure gradient. As shown in Fig. 8(a), similar trends are found in S0, S1, and S2: Lifespan increases with the increase of L_w and decrease of dP , which makes sense according to Darcy's law. Contour lines indicate that lifespan is almost equally sensitive to dP and L_w at the left top corner of the 2D parameter space ($dP < 10$ MPa, $L_w > 700$ m). The sensitivity of lifespan to L_w decreases slightly as L_w is shortened, and the impact of dP on lifespan is significantly reduced when dP increases over 10 MPa. It suggests that lifespan is mainly controlled by L_w for larger pressure gradients. The comparison of three response surfaces also reveals that lifespan is shorter, with stronger heterogeneity

in sequence of S0, S1 and S2.

The comparison of lifespan is extended to all scenarios at every dP - L_w sample point in Fig. 9(a). The lifespan variance between S0-S6 increases with its values at the sample points, though the order of the value is the same at every point: $S0 > S3 \approx S5 > S1 > S6 > S4 > S2$. The comparison of lifespan values between scenarios is shown most clearly at Sample#1 ($dP = 5.19$ MPa, $L_w = 983$ m) with the highest lifespan values, which will be taken as an example for the following lifespan analysis. S0 and S2 have the highest and lowest lifespan, i.e., 73 and 49.5 years, respectively, as the homogeneous and most heterogeneous scenario. It is because preferential CO_2 flow

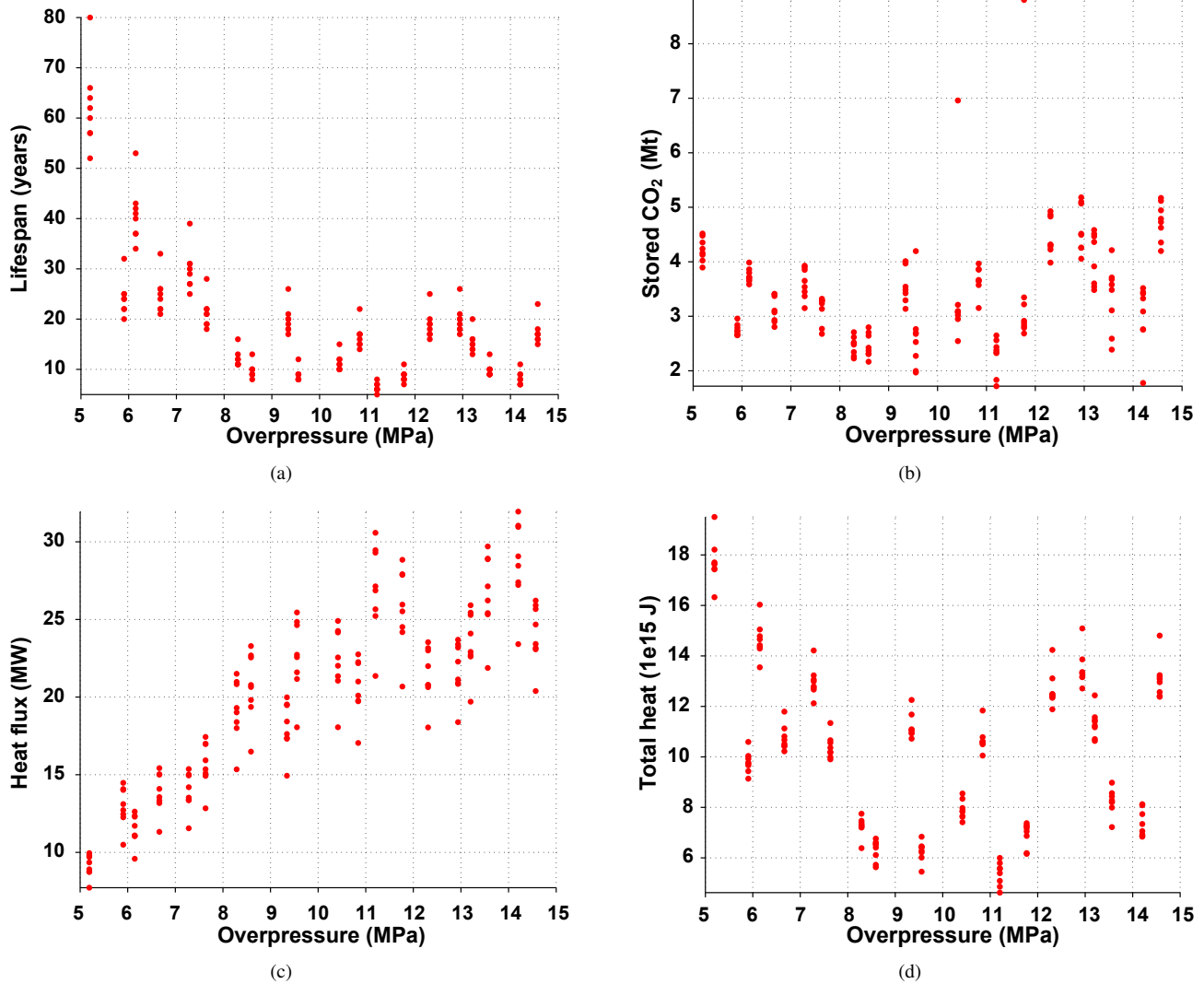


Fig. 7. Scatterplots of (a) lifespan, (b) stored CO₂ mass, (c) produced heat flux, and (d) total produced heat energy corresponding to dP for all the 160 model simulations of S1.

is more significant in the stronger heterogeneous field. Cold CO₂ will follow the preferential path to the production wells and bypass low-permeable hot areas, causing earlier cold fluid breakthrough and lower heat-sweeping efficiency.

S1-S5 have the same degree of heterogeneity (variance = 0.002) but different correlation length or azimuth. S4 stands out with the notable lower lifespan (58 years) than the other 4 scenarios. The direction of maximum continuity is x ($CL_x = 800$ m), and the minimum direction is y ($CL_y = 200$ m), resulting a horizontal anisotropy ratio of 4. This configuration of geostatistical model generates high and low-permeable lenses in parallel to flow directions (x -axis). It helps to develop the shortest preferential flow paths between IW and PWs, leading to earlier cold front breakthrough than the other 4 scenarios. In contrast, the 800-m long lenses in S5 are perpendicular to flow directions and in parallel to 1-km long horizontal wells, and hence the low-permeable lenses serve as flow barriers, resulting in a lifespan (63.625 years) even longer than S1's (62.25 years). S6, with lens rotated 45°

horizontally (azimuth = 45°) from S5, turns out a lifespan of 61.5 years, which is between that of S4 and S5. These results suggest in an anisotropic field, the azimuth of horizontal wells should be optimized to avoid either shortest preferential paths or largest flow barriers in order to achieve heat production goals. S3 with isotropic but shorter correlation lengths (200 m in both x and y -axis) leads to slightly longer lifespan than S1 (63.75 vs. 62.25 years). The smaller-scale heterogeneity in S3 generates more tortuous preferential flow paths, slowing down the cold CO₂ flow to PWs and increasing the heat sweeping area.

3.2.2 Stored CO₂ and produced heat energy during lifespan

Fig. 8(b) presents the response surfaces of total stored CO₂ (net injected) in lifespan in dP - L_w parameter space in S0-S2. It is mainly controlled by L_w and increased almost linearly with L_w , as longer L_w means larger pore volume for CO₂ storage. More CO₂ mass can be compressed to store

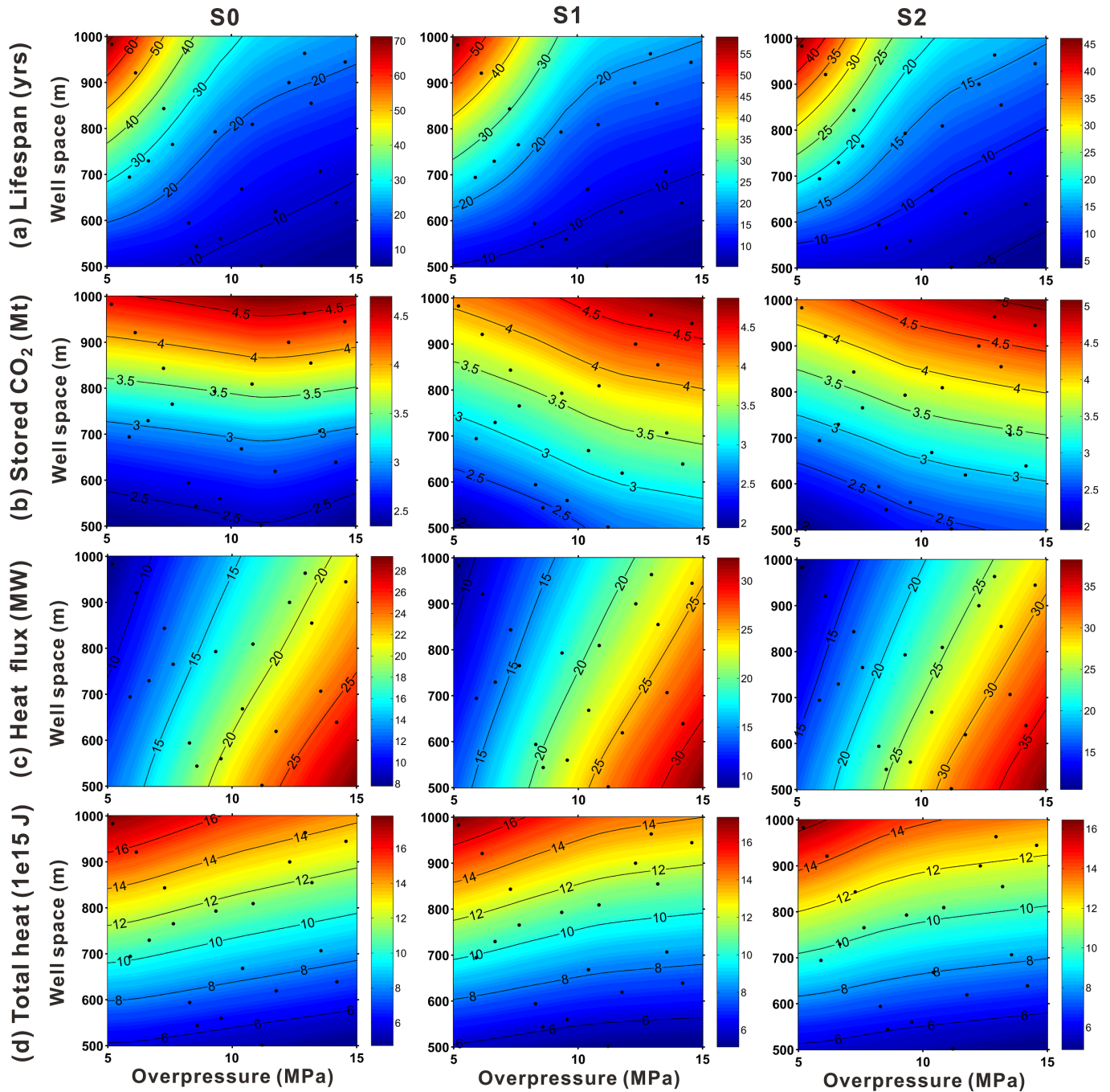


Fig. 8. Response surfaces of (a) lifespan, (b) stored CO₂ mass, (c) produced heat flux, and (d) total produced heat energy corresponding to dP - L_w for S0, S1, and S2. Mean values of the 8 realizations are used for S1 and S2. Solid black dots represent the 20 dP - L_w sample points.

in pore space under higher dP to some extent. The impact of dP on CO₂ storage seems stronger in S1 and S2 than in S0. In addition, when $dP > 12$ MPa, CO₂ storage continues to increase with dP in S1 and S2, but in S0 it reverses to decrease with dP slightly, which could lead to a large gap between S0 and heterogeneous scenarios near upper limit of dP . Fig. 9(b) shows at the Sample# 5 and 16 with the top two dP (14.20 and 14.57 MPa), stored CO₂ mass in S0 is less than that from all the heterogeneous scenarios by over 0.5 Mt. It is also noted that S3 stands out with the highest storage with

> 1 -Mt above S0 in these 2 samples and Sample# 15 ($dP = 13.56$ MPa). These results suggest that heterogeneity of the porosity field, especially smaller scales, helps to store more CO₂ under higher pressures.

The average produced heat flux in lifespan time is affected significantly by dP and moderately by L_w (Fig. 8(c)). As a product of mass flux and specific enthalpy, it is positively correlated to CO₂ circulation rate, which increases with dP and decreases with L_w . The distribution pattern versus dP - L_w is generally reverse to that of lifespan, suggesting that

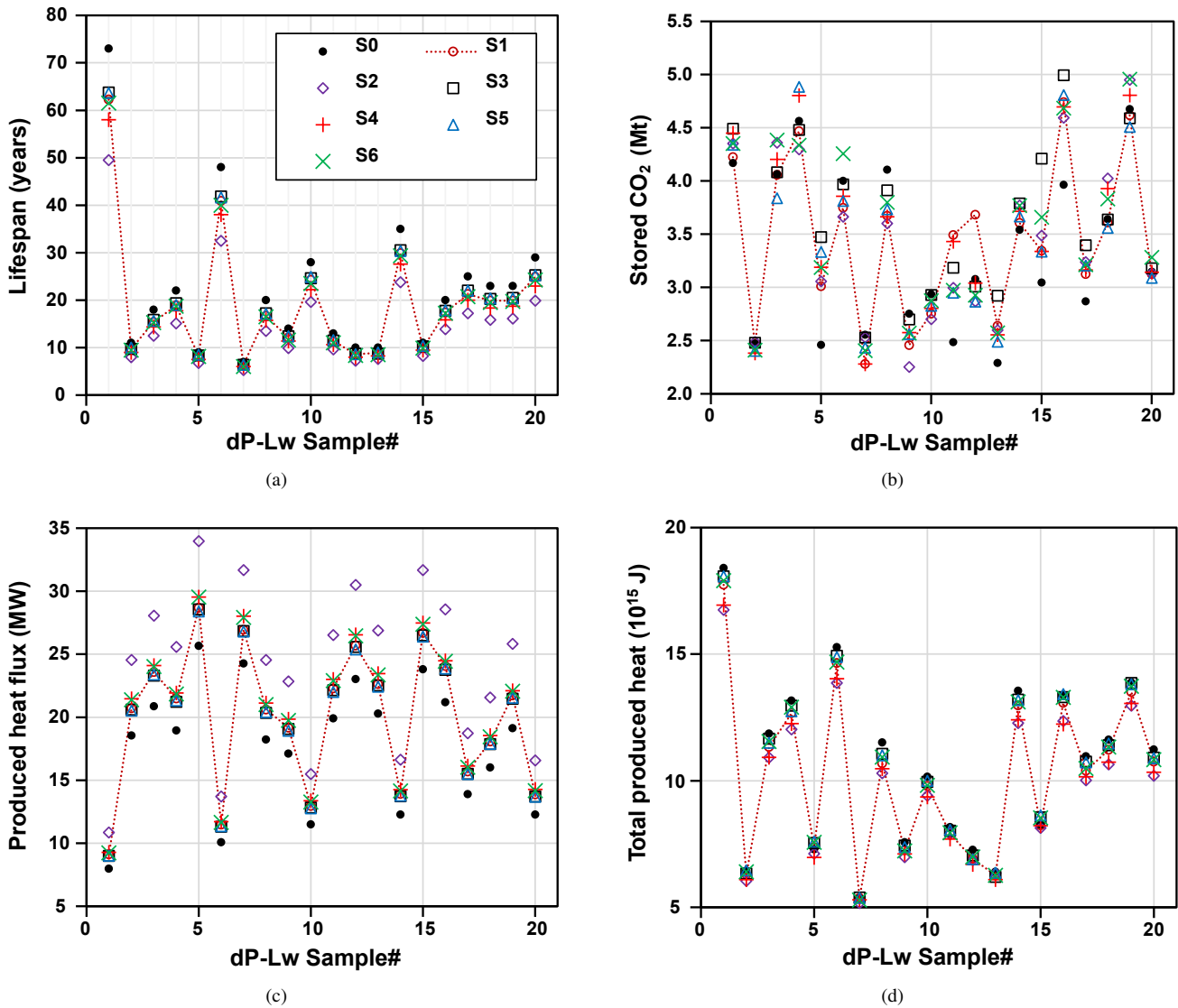


Fig. 9. Comparison of (a) lifespan, (b) stored CO₂ mass, (c) produced heat flux, and (d) total produced heat energy in lifespan between S0-S6 for each *dP-Lw* sample input. The values are the mean of the eight realizations for heterogeneous scenarios S1-S6. The 20 *dP-Lw* sample values are listed in Table 2.

higher produced heat flux leads to shorter lifespan. In other words, there is a tradeoff between the power plant capacity and lifespan in a given geothermal reservoir. As indicated in Fig. 9(c), both sequences of heat flux values between Sample# 1-20 and between S0-S6 are reversed to those of lifespan. As heat flux and lifespan are dependent on CO₂ mass flux positively and negatively, interpretations of interplay of heterogeneity and *dP-Lw* on heat flux are similar to those for lifespan in the last sub-section.

The total heat energy recovered in lifespan is cumulative products of heat flux and lifespan in each time step but the overall distribution with *dP-Lw* is prone to that of lifespan. As shown in Fig. 8(d), it decreases slightly with *dP* and increases significantly with *Lw*, almost linearly according to contour line spaces. The values between S0-S6 follow the same order as lifespan, but gaps between them are downscaled, considering the counteractive effect from heat flux (Fig. 9(d)). Produced

heat flux and the total heat recovered are mainly controlled by *dP* and *Lw*, respectively. Although higher *dP* comes with higher circulation rate and produced heat flux, it leads to lower total heat recovered, especially with shorter *Lw* in more heterogeneous formations.

4. Conclusions and future studies

A suite of numerical simulations is conducted on a set of horizontal well-triplet placements with a range of well space and overpressure to circulate CO₂ in a set of heterogeneous geothermal reservoirs with various heterogeneity characteristics (variance, correlation length, anisotropy, and azimuth). Four performance indicators, i.e., lifespan, stored CO₂ mass, produced heat flux, total recovered heat energy, are used to evaluate geothermal productions in these simulations, and how they are affected by the reservoir heterogeneity, well space, and pressure. The main findings and conclusions are drawn as

follows:

- Stronger heterogeneity (S2) field generates more prominent preferential CO₂ flow paths, causing earlier cold CO₂ breakthrough in production wells, lower heat-sweeping efficiency shorter lifespan of geothermal reservoirs, higher produced heat flux averaged in lifespan, and lower total heat recovered in lifespan. Whereas heterogeneity has a minor impact on the stabilized CO₂ storage rate after 5 years of circulation.
- Isotropic heterogeneous field with shorter correlation length (S3) produces more tortuous preferential CO₂ flow paths, which slows down the cold CO₂ breakthrough, increases the heat-sweeping area, and leads to a lifespan longer than any other heterogeneous scenarios (S1, S2, S4, S5, S6). Under high pressures, CO₂ is stored more in S3 than in other scenarios, and significantly less in homogeneous case (S0).
- Anisotropy of the heterogeneous fields plays an important role in our particular horizontal well-triplet placement. When the direction of maximum continuity is parallel to major flow direction x , i.e., perpendicular to horizontal wells, the high-permeable lenses serve as straight preferential flow paths (S4). In contrast, when the maximum continuity is perpendicular to x (parallel to horizontal wells), the low-permeable lenses become flow barriers between IW and PW (S5). Additionally, S6, with direction of maximal continuity rotated 45° horizontally, is a tradeoff between S4 and S5. Consequently, in a sequence of S4, S6, S5, lifespan is getting longer, produced heat flux is lower, and total recovered heat becomes more. However, the impact of anisotropy is not that strong as that of heterogeneity variance.
- Lifespan is almost equally sensitive to dP and L_w . Net stored CO₂ is mainly controlled by L_w only, because it defined the sweeping area. Produced heat flux is controlled by dP , while total recovered heat is dominated by L_w . Higher dP leads to higher heat flux, but recovers less total heat, especially with shorter L_w in more heterogeneous scenarios.

In this study, the heterogeneous reservoirs are assumed filled with CO₂ initially, which is not a realistic reservoir state. Future works may include sequential CO₂ sequestration and circulation, in which heterogeneity will play a more significant role in CO₂ migration, storage, and associated geothermal recovery. Moreover, optimization of well space and operation overpressure is very much needed to achieve maximum heat recovery or economic profit for heterogeneous reservoir systems. Only two different values of each geostatistical parameter are used for comparison analysis, future work may obtain continuous values sampled in a defined range for global sensitivity analysis of these geostatistical parameters.

Acknowledgement

This work is funded by grants #IG/DVC/WRC/22/02 and #RC/RG-DVC/WRC/21/02. Supports from the research group DR/RG/17 of Sultan Qaboos University are appreciated.

Conflict of interest

The authors declare no competing interest.

Open Access This article is distributed under the terms and conditions of the Creative Commons Attribution (CC BY-NC-ND) license, which permits unrestricted use, distribution, and reproduction in any medium, provided the original work is properly cited.

References

- Abas, N., Khan, N. Carbon conundrum, climate change, CO₂ capture and consumptions. *Journal of CO₂ Utilization*, 2014, 8: 39-48.
- Abbaszadeh, M., Koide, N., Murahashi, Y. Integrated characterization and flow modeling of a heterogeneous carbonate reservoir in Daleel field, Oman. *SPE Reservoir Evaluation & Engineering*, 2000, 3(2): 150-159.
- Adams, B. M., Kuehn, T. H., Bielicki, J. M., et al. On the importance of the thermosiphon effect in CPG (CO₂ plume geothermal) power systems. *Energy*, 2014, 69: 409-418.
- Adams, B. M., Kuehn, T. H., Bielicki, J. M., et al. A comparison of electric power output of CO₂ plume geothermal (CPG) and brine geothermal systems for varying reservoir conditions. *Applied Energy*, 2015, 140: 365-377.
- Al-Lamki, M., Terken, J. M. The role of hydrogeology in Petroleum Development Oman. *GeoArabia*, 1996, 1(4): 495-510.
- Atrens, A. D., Gurgenci, H., Rudolph, V. CO₂ thermosiphon for competitive geothermal power generation. *Energy & Fuels*, 2009, 23(1): 553-557.
- Buscheck, T. A., Bielicki, J. M., Chen, M., et al. Integrating CO₂ storage with geothermal resources for dispatchable renewable electricity. *Energy Procedia*, 2014, 63: 7619-7630.
- Buscheck, T. A., Elliot, T. R., Celia, M. A., et al. Integrated geothermal-CO₂ reservoir systems: Reducing carbon intensity through sustainable energy production and secure CO₂ storage. *Energy Procedia*, 2013, 37: 6587-6594.
- Buscheck, T. A., Sun, Y., Chen, M., et al. Active CO₂ reservoir management for carbon storage: Analysis of operational strategies to relieve pressure buildup and improve injectivity. *International Journal of Greenhouse Gas Control*, 2012, 6: 230-245.
- Chen, M., Abdalla, O., Izady, A., et al. Development and surrogate-based calibration of a CO₂ reservoir model. *Journal of Hydrology*, 2020, 586: 124698.
- Chen, M., Al-Maktoumi, A., Izady, A. Assessment of integrated CO₂ geologic storage and geothermal harvest in a semi-closed thin reservoir. *Sustainable Energy Technologies and Assessments*, 2022, 49: 101773.
- Chen, M., Al-Maktoumi, A., Rajabi, M. M., et al. Evaluation of CO₂ sequestration and circulation in fault-bounded thin geothermal reservoirs in North Oman using response surface methods. *Journal of Hydrology*, 2021, 598: 126411.
- Crooijmans, R., Willems, C., Nick, H., et al. The influence of facies heterogeneity on the doublet performance in low-enthalpy geothermal sedimentary reservoirs. *Geother-*

- mics, 2016, 64: 209-219.
- Dai, Z., Middleton, R., Viswanathan, H., et al. An integrated framework for optimizing CO₂ sequestration and enhanced oil recovery. *Environmental Science & Technology Letters*, 2014, 1(1): 49-54.
- Ershadnia, R., Wallace, C. D., Hajirezaie, S., et al. Hydrothermo-chemo-mechanical modeling of carbon dioxide injection in fluvial heterogeneous aquifers. *Chemical Engineering Journal*, 2022, 431: 133451.
- GCCSI. *The Global Status of CCS, Summary Report*, Global Carbon Capture and Storage Institute, 2014.
- Hao, Y., Sun, Y., Nitao, J. J. Overview of NUFT: A versatile numerical model for simulating flow and reactive transport in porous media, in *Groundwater Reactive Transport Models*, edited by F. Zhang, G. Yeh, and J. C. Parker, Bentham Science Publisher, United Arab Emirates, pp. 212-239, 2012.
- Harris, C., Jackson, S. J., Benham, G. P., et al. The impact of heterogeneity on the capillary trapping of CO₂ in the Captain Sandstone. *International Journal of Greenhouse Gas Control*, 2021, 112: 103511.
- IPCC (Intergovernmental Panel on Climate Change). *IPCC Special Report on Carbon Dioxide Capture and Storage*. Cambridge University Press, New York, USA, 2005.
- Liu, G., Pu, H., Zhao, Z., et al. Coupled thermo-hydro-mechanical modeling on well pairs in heterogeneous porous geothermal reservoirs. *Energy*, 2019, 171: 631-653.
- Mac Dowell, N., Fennell, P. S., Shah, N., et al. The role of CO₂ capture and utilization in mitigating climate change. *Nature Climate Change*, 2017, 7: 243-249.
- McKay, M. D., Beckman, R. J., Conover, W. J. A comparison of three methods for selecting values of input variables in the analysis of output from a computer code. *Technometrics*, 1979, 21(2): 239-245.
- Nitao, J. J. Reference manual for the NUFT flow and transport code, version 2.0. Technical Report UCRL-MA-130651. Lawrence Livermore National Laboratory, Livermore, CA, 1998.
- Randolph, J. B., Saar, M. O. Coupling carbon dioxide sequestration with geothermal energy capture in naturally permeable, porous geologic formations: Implications for CO₂ sequestration. *Energy Procedia*, 2011, 4: 2206-2213.
- Rasheed, Z., Raza, A., Gholami, R., et al. A numerical study to assess the effect of heterogeneity on CO₂ storage potential of saline aquifers. *Energy Geoscience*, 2020, 1(1-2): 20-27.
- Ren, J., Wang, Y., Feng, D., et al. CO₂ migration and distribution in multiscale-heterogeneous deep saline aquifers. *Advances in Geo-Energy Research*, 2021, 5(3): 333-346.
- Saar, M. O., Buscheck, T. A., Jenny, P., et al. Numerical study of multi-fluid and multi-level geothermal system performance. Paper Presented at Proceedings World Geothermal Congress 2015, Melbourne, Australia, 19-25 April, 2015.
- Schütz, F., Winterleitner, G., Huenges, E. Geothermal exploration in a sedimentary basin: New continuous temperature data and physical rock properties from northern Oman. *Geothermal Energy*, 2018, 6: 5.
- Shaffer, G. Long-term effectiveness and consequences of carbon dioxide sequestration. *Nature Geoscience*, 2010, 3: 464-467.
- Sohal, M. A., Le Gallo, Y., Audigane, P., et al. Effect of geological heterogeneities on reservoir storage capacity and migration of CO₂ plume in a deep saline fractured carbonate aquifer. *International Journal of Greenhouse Gas Control*, 2021, 108: 103306.
- Sun, F., Yao, Y., Li, G., et al. Performance of geothermal energy extraction in a horizontal well by using CO₂ as the working fluid. *Energy Conversion and Management*, 2018, 171: 1529-1539.
- Willems, C. J., Nick, H. M., Donselaar, M. E., et al. On the connectivity anisotropy in fluvial hot sedimentary aquifers and its influence on geothermal doublet performance. *Geothermics*, 2017, 65: 222-233.
- Williams, G. A., Chadwick, R. A. Influence of reservoir-scale heterogeneities on the growth, evolution and migration of a CO₂ plume at the Sleipner Field, Norwegian North Sea. *International Journal of Greenhouse Gas Control*, 2021, 106: 103260.
- Xu, T., Tian, H., Zhu, H., et al. China actively promotes CO₂ capture, utilization and storage research to achieve carbon peak and carbon neutrality. *Advances in Geo-Energy Research*, 2022, 6(1): 1-3.
- Zhang, L., Zhou, L., Al-Mugheiry, M., et al. Horizontal water flooding in Shuaiba carbonate reservoir of Daleel Field in Oman: From pilots' performance to development era. Paper SPE-108392-MS Presented at SPE Annual Technical Conference and Exhibition, Anaheim, California, 11-14 November, 2007.
- Zhao, G., Mu, L., Wu, X. The application of horizontal wells in effectively developing thinly-bedded carbonate reservoirs of block 5, Oman. Paper Presentation at AAPG Annual Convention and Exhibition, Long Beach, California, 22-25 April, 2012.